

SQUID Metamaterials on a Lieb lattice: From flat-band to nonlinear localization

N. Lazarides^{1,2,3,4}, G. P. Tsironis^{1,2,3,4}

¹*Department of Physics, University of Crete, P. O. Box 2208, 71003 Heraklion, Greece;*

²*Institute of Electronic Structure and Laser, Foundation for Research and Technology–Hellas, P.O. Box 1527, 71110 Heraklion, Greece*

³*National University of Science and Technology "MISiS", Leninsky prosp. 4, Moscow, 119049, Russia;*

⁴*Department of Physics, School of Science and Technology, Nazarbayev University, 53 Kabanbay Batyr Ave., Astana 010000, Kazakhstan*

(Dated: September 20, 2018)

The dynamic equations for the fluxes through the SQUIDs that form a two-dimensional metamaterial on a Lieb lattice are derived, and then linearized around zero flux to obtain the *linear frequency spectrum* according to the standard procedure. That spectrum, due to the Lieb lattice geometry, possesses a frequency band structure exhibiting two characteristic features; two dispersive bands, which form a Dirac cone at the corners of the first Brillouin zone, and a flat band crossing the Dirac points. It is demonstrated numerically that localized states can be excited in the system when it is initialized with single-site excitations; depending on the amplitude of those initial states, the localization is either due to the flat-band or to nonlinear effects. Flat-band localized states are formed in the nearly linear regime, while localized excitations of the discrete breather type are formed in the nonlinear regime. These two regimes are separated by an intermediate turbulent regime for which no localization is observed. Notably, initial single-site excitations of only edge SQUIDs of a unit cell may end-up in flat-band localized states; no such states are formed for initial single-site excitations of a corner SQUID of a unit cell. The degree of localization of the resulting states is in any case quantified using well-established measures such as the energetic participation ratio and the second moment.

PACS numbers: 63.20.Pw, 11.30.Er, 41.20.-q, 78.67.Pt

Keywords: SQUID metamaterials, Lieb lattice, flat dispersion bands, localized flat-band states, Hamiltonian systems, Discrete breathers

I. INTRODUCTION

Considerable research effort has focused the last two decades in the investigation and development of artificial mediums or *metamaterials*, which exhibit properties not found in natural materials^{1–6}. After the development of active, tunable, and nonlinear metamaterials^{7,8}, those artificial mediums are expected to have a strong impact across the entire range of technologies where electromagnetic radiation is used. Moreover, they may provide a flexible platform for modeling and mimicking fundamental physical effects^{9–11}. An important class of metamaterials is that of superconducting ones^{12,13}, and in particular those comprising Superconducting QUantum Interference Devices (SQUIDs). The idea of a metamaterial consisting of SQUIDs was theoretically introduced about a decade ago both in the quantum¹⁴ and the classical regimes¹⁵.

The simplest version of a SQUID consists of a superconducting ring interrupted by a Josephson junction¹⁶, as shown schematically in Fig. 1. The SQUIDs are highly nonlinear devices, exhibiting strong resonant response to applied magnetic fields. SQUID metamaterials in one and two dimensions have been realized and investigated in the laboratory, and they were found to exhibit novel properties such as negative diamagnetic permeability^{17,18}, broad-band tunability^{18,19}, self-induced broad-band transparency²⁰, as well as dynamic multistability and switching²¹, among others. Some of

these properties, i.e., dynamic multistability and tunability, have been also revealed in numerical simulations^{22,23}. Moreover, nonlinear localization²⁴ and the emergence of counter-intuitive dynamic states referred to as *chimera states* in current literature^{25,26} have been demonstrated numerically in SQUID metamaterial models.

The notion of metamaterials implies the freedom to engineer not only the properties of the individual "particles" or devices which play the role of "atoms" in an artificial medium, but also their arrangement in space, i.e., the type of the lattice. Remarkably, some specific lattice geometries such as those of *Lieb* or *Kagomé* lattices give rise to novel and potentially useful band structures. The former is a square-depleted (line-centered tetragonal) lattice, described by three sites in a square unit cell as illustrated in Fig. 2. It is characterized by a band structure featuring Dirac cones intersected by a topological flat band. Localization on flat-bands has been extensively investigated in relatively simple lattice models^{27,28}, even in the presence of disorder^{29,30}. Superpositions of flat-band modes and their stability have been also investigated in rhombic nonlinear optical waveguide arrays³¹. The Lieb lattice was first introduced in the context of photonics in Ref.³². Recently, photonic Lieb lattices have been experimentally realized and the existence of localized flat-band modes has been reported^{33,34}. The world of electronic flat-band systems has been reviewed in a recent article³⁵. Moreover, electronic Lieb lattices have been experimentally realized and characterized³⁶. Here, a SQUID metamaterial on a Lieb lattice is considered,

in which each site is occupied by a SQUID. In each unit cell, two of the SQUIDs (indicated in red and blue) are neighbored by two other SQUIDs. The third SQUID in the unit cell (black) has four neighbors. In what follows, these SQUIDs will be referred to as edge SQUIDs (red and blue) and corner (black) SQUID, respectively.

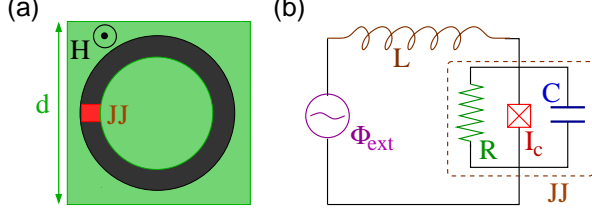


FIG. 1: (Color online) Schematic of a SQUID (a) and its equivalent electrical circuit (b).

In the following, the dynamical equations for the fluxes through the SQUIDs and the linear frequency spectrum are obtained for a SQUID Lieb metamaterial (SLiMM). Using numerical simulations, the generation of *localized flat band states* when a single edge SQUID is initially excited at low amplitude, is demonstrated. No flat-band localization is observed when single corner SQUIDs are initially excited at low amplitudes, in agreement with the experiments in optical Lieb lattices^{33,34,37}. For high-amplitude initial excitations of either a corner or an edge SQUID, nonlinear localization of the discrete breather type is observed³⁸. The cross-over between flat-band and nonlinear localization is explored; the two regimes are clearly separated by an intermediate, no-localization regime. Thus, flat-band localized states cannot be continued into the nonlinearly localized ones of the discrete breather or discrete soliton type, as it has been demonstrated for discrete nonlinear Schrödinger type models of various flat-band lattices and ribbons^{29,39–43}.

II. FLUX DYNAMICS

Consider the Lieb lattice of Fig. 2, in which each site is occupied by a SQUID. That SLiMM can be regarded as the combination of three sublattices colored as blue, red, and black. All the SQUIDs are identical, and they are magnetically coupled to their nearest neighbors through their mutual inductances. In order to derive the dynamic equations for the fluxes through the SQUIDs of the SLiMM, we first write the flux-balance relations for all SQUIDs

$$\begin{aligned}\Phi_{n,m}^A &= \Phi_{ext} + L \{ I_{n,m}^A + \lambda_x [I_{n-1,m}^B + I_{n,m}^B] \\ &\quad + \lambda_y [I_{n,m-1}^C + I_{n,m}^C] \}, \\ \Phi_{n,m}^B &= \Phi_{ext} + L \{ I_{n,m}^B + \lambda_x [I_{n,m}^A + I_{n+1,m}^A] \}, \\ \Phi_{n,m}^C &= \Phi_{ext} + L \{ I_{n,m}^C + \lambda_y [I_{n,m}^A + I_{n,m+1}^A] \},\end{aligned}\quad (1)$$

where $I_{n,m}^k$ is the current in the SQUID of the (n, m) th unit cell of kind k ($k = A, B, C$), Φ_{ext} is the applied

(external) flux, and $\lambda_x = M_x/L$ ($\lambda_y = M_y/L$) is the coupling coefficient along the horizontal (vertical) direction, with M_x (M_y) being the corresponding mutual inductance between neighboring SQUIDs and L the self-inductance of each SQUID. The current in each SQUID is given by the resistively and capacitively shunted junction (RCSJ) model⁴⁴, as

$$-I_{n,m}^k = C \frac{d^2 \Phi_{n,m}^k}{dt^2} + \frac{1}{R} \frac{d \Phi_{n,m}^k}{dt} + I_c \sin \left(2\pi \frac{\Phi_{n,m}^k}{\Phi_0} \right), \quad (2)$$

where R is the quasiparticle resistance through the Josephson junction of each SQUID, C is the capacitance of each SQUID, and I_c is the critical current of the Josephson junction of each SQUID. Then Eqs. (1) are inverted to obtain the currents $I_{n,m}^k$ as functions of the fluxes $\Phi_{n,m}^k$. By substitution of the obtained currents back into Eqs. (1), and neglecting all the terms which are proportional to $\lambda_x^a \lambda_y^b$ with $a + b > 1$, we get

$$\begin{aligned}L I_{n,m}^A &= \Phi_{n,m}^A - \lambda_x (\Phi_{n,m}^B + \Phi_{n-1,m}^B) \\ &\quad - \lambda_y (\Phi_{n,m}^C + \Phi_{n,m-1}^C) - \Phi_{eff}^A, \\ L I_{n,m}^B &= \Phi_{n,m}^B - \lambda_x (\Phi_{n,m}^A + \Phi_{n+1,m}^A) - \Phi_{eff}^B, \\ L I_{n,m}^C &= \Phi_{n,m}^C - \lambda_y (\Phi_{n,m}^A + \Phi_{n,m+1}^A) - \Phi_{eff}^C,\end{aligned}\quad (3)$$

where $\Phi_{eff}^A = [1 - 2(\lambda_x + \lambda_y)]\Phi_{ext}$, $\Phi_{eff}^B = (1 - 2\lambda_x)\Phi_{ext}$, and $\Phi_{eff}^C = (1 - 2\lambda_y)\Phi_{ext}$ are the "effective" external fluxes. Combining Eqs. (2) and (3) we get

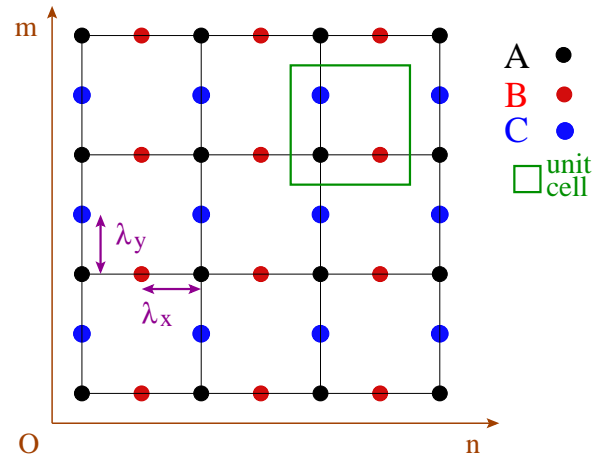


FIG. 2: (Color online) Schematic of a Lieb lattice in which each site is occupied by a SQUID. The three sublattices are indicated in black (corner SQUIDs), red (edge SQUIDs), and blue (edge SQUIDs) color. The nearest-neighbor couplings along the horizontal (λ_x) and vertical (λ_y) directions and the unit cell are also indicated.

$$\begin{aligned}
& LC \frac{d^2 \Phi_{n,m}^A}{dt^2} + \frac{L}{R} \frac{d\Phi_{n,m}^A}{dt} + LI_c \sin \left(2\pi \frac{\Phi_{n,m}^A}{\Phi_0} \right) + \Phi_{n,m}^A \\
&= \lambda_x (\Phi_{n,m}^B + \Phi_{n-1,m}^B) + \lambda_y (\Phi_{n,m}^C + \Phi_{n,m-1}^C) + \Phi_{eff}^A, \\
& LC \frac{d^2 \Phi_{n,m}^B}{dt^2} + \frac{L}{R} \frac{d\Phi_{n,m}^B}{dt} + LI_c \sin \left(2\pi \frac{\Phi_{n,m}^B}{\Phi_0} \right) + \Phi_{n,m}^B \\
&= \lambda_x (\Phi_{n,m}^A + \Phi_{n+1,m}^A) + \Phi_{eff}^B, \quad (4) \\
& LC \frac{d^2 \Phi_{n,m}^C}{dt^2} + \frac{L}{R} \frac{d\Phi_{n,m}^C}{dt} + LI_c \sin \left(2\pi \frac{\Phi_{n,m}^C}{\Phi_0} \right) + \Phi_{n,m}^C \\
&= \lambda_y (\Phi_{n,m}^A + \Phi_{n,m+1}^A) + \Phi_{eff}^C.
\end{aligned}$$

Using the relations

$$\tau = \omega_{LC} t, \quad \phi_{n,m}^k = \frac{\Phi_{n,m}^k}{\Phi_0}, \quad \phi_{ext} = \frac{\Phi_{ext}}{\Phi_0}, \quad (5)$$

where $\omega_{LC} = 1/\sqrt{LC}$ is the inductive-capacitive SQUID frequency, the dynamic equations for the fluxes through the SQUIDs can be written in the normalized form

$$\begin{aligned}
& \ddot{\phi}_{n,m}^A + \gamma \dot{\phi}_{n,m}^A + \beta \sin(2\pi \phi_{n,m}^A) + \phi_{n,m}^A \\
&= \lambda_x (\phi_{n,m}^B + \phi_{n-1,m}^B) + \lambda_y (\phi_{n,m}^C + \phi_{n,m-1}^C) + \phi_{eff}^A, \\
& \ddot{\phi}_{n,m}^B + \gamma \dot{\phi}_{n,m}^B + \beta \sin(2\pi \phi_{n,m}^B) + \phi_{n,m}^B \\
&= \lambda_x (\phi_{n,m}^A + \phi_{n+1,m}^A) + \phi_{eff}^B, \quad (6) \\
& \ddot{\phi}_{n,m}^C + \gamma \dot{\phi}_{n,m}^C + \beta \sin(2\pi \phi_{n,m}^C) + \phi_{n,m}^C \\
&= \lambda_y (\phi_{n,m}^A + \phi_{n,m+1}^A) + \phi_{eff}^C,
\end{aligned}$$

where

$$\beta = \frac{LI_c}{\Phi_0} \quad \text{and} \quad \gamma = \omega_{LC} \frac{L}{R}, \quad (7)$$

is the SQUID parameter and the loss coefficient, respectively, and ϕ_{eff}^k are the normalized effective fluxes. The overdots on $\phi_{n,m}^k$ denote differentiation with respect to the normalized temporal variable τ . The values of the fluxes through the SQUIDs $\phi_{n,m}^k$ generally depend on k . Suppose that $\gamma = 0$ and $\phi_{ext} = 0$, and that Eqs. (6) are initialized with a low amplitude homogeneous excitation, i.e., with $\phi_{n,m}^k = c$ for any n, m , and k ($c \ll 1$ is a constant). After integrating Eqs. (6) in time assuming periodic boundary conditions, at the steady state, the fluxes through the SQUIDs of the same kind will be the same. However, the fluxes through the SQUIDs of different kind will be different. This is due to the Lieb lattice geometry and the (generally) different values of λ_x and λ_y , since the flux through a particular SQUID of the SLiMM depends not only on the self-induced one, but also on the fluxes from the SQUIDs to which that particular SQUID is coupled (four for A SQUIDs and two for B and C SQUIDs). Moreover, the coupling between SQUIDs is proportional to the coefficients λ_x or λ_y . Note that for isotropic coupling, $\lambda_x = \lambda_y$, the fluxes through the SQUIDs of kind B and C are the same but different than those through the SQUIDs of kind A ($\phi_{n,m}^B = \phi_{n,m}^C \neq \phi_{n,m}^A$).

In the following, we are concerned about energy-conserving SLiMMs, i.e., about the Hamiltonian version of SQUID Lieb metamaterials, and thus we set $\gamma = 0$ and $\phi_{ext} = 0$ into Eqs. (6).

III. LINEAR FREQUENCY SPECTRUM

Without losses and driving forces, Eqs. (6) are linearized using the relation $\beta \sin(2\pi \phi_{n,m}^k) \simeq \beta_L \phi_{n,m}^k$, where $\beta_L = 2\pi\beta$. Thus we get

$$\begin{aligned}
& \ddot{\phi}_{n,m}^A + \Omega_{SQ}^2 \phi_{n,m}^A = \lambda_x (\phi_{n,m}^B + \phi_{n-1,m}^B) \\
& \quad + \lambda_y (\phi_{n,m}^C + \phi_{n,m-1}^C), \\
& \ddot{\phi}_{n,m}^B + \Omega_{SQ}^2 \phi_{n,m}^B = \lambda_x (\phi_{n,m}^A + \phi_{n+1,m}^A), \quad (8) \\
& \ddot{\phi}_{n,m}^C + \Omega_{SQ}^2 \phi_{n,m}^C = \lambda_y (\phi_{n,m}^A + \phi_{n,m+1}^A),
\end{aligned}$$

where $\Omega_{SQ} = \sqrt{1 + \beta_L}$ is the resonance frequency of individual SQUIDs in the linear limit. In order to obtain the linear frequency spectrum, we substitute into the linearized Eqs. (8) the plane wave solution

$$\phi_{n,m}^k = \mathcal{F}_k \exp[i(\Omega\tau - \kappa_x n - \kappa_y m)], \quad (9)$$

where κ_x and κ_y are the x and y components of the two-dimensional, normalized wavevector κ , and $\Omega = \omega/\omega_{LC}$ is the normalized frequency. After some calculations we get

$$\begin{aligned}
& (\Omega_{SQ}^2 - \Omega^2) \mathcal{F}_A - \lambda_x (1 + e^{+i\kappa_x}) \mathcal{F}_B \\
& \quad - \lambda_y (1 + e^{+i\kappa_y}) \mathcal{F}_C = 0, \\
& -\lambda_x (1 + e^{-i\kappa_x}) \mathcal{F}_A + (\Omega_{SQ}^2 - \Omega^2) \mathcal{F}_B = 0, \quad (10) \\
& -\lambda_y (1 + e^{-i\kappa_y}) \mathcal{F}_A + (\Omega_{SQ}^2 - \Omega^2) \mathcal{F}_C = 0.
\end{aligned}$$

In order to obtain nontrivial solutions for the amplitudes \mathcal{F}_k of the stationary problem Eqs. (10), its determinant \mathcal{D} should be equal to zero, i.e.,

$$\begin{aligned}
& \mathcal{D} = (\Omega_{SQ}^2 - \Omega^2) \left\{ (\Omega_{SQ}^2 - \Omega^2)^2 \right. \\
& \quad \left. - 4 \left[\lambda_x^2 \cos^2 \left(\frac{\kappa_x}{2} \right) + \lambda_y^2 \cos^2 \left(\frac{\kappa_y}{2} \right) \right] \right\} = 0. \quad (11)
\end{aligned}$$

Solving Eq. (11) for $\Omega \equiv \Omega_\kappa$, we get

$$\begin{aligned}
& \Omega_\kappa = \Omega_{SQ}, \quad (12) \\
& \Omega_\kappa = \sqrt{\Omega_{SQ}^2 \pm 2\sqrt{\lambda_x^2 \cos^2 \left(\frac{\kappa_x}{2} \right) + \lambda_y^2 \cos^2 \left(\frac{\kappa_y}{2} \right)}} \quad (13)
\end{aligned}$$

where only positive frequencies are considered. Eqs. (12) and (13) provide the *linear frequency spectrum of the SLiMM*. Thus, the Lieb lattice geometry possesses a frequency band structure exhibiting two characteristic features as can be observed in Fig. 3: two dispersive bands, which form a Dirac cone at the corners of the first Brillouin zone (for $\kappa_x = \kappa_y = \pm\pi$), and a flat band crossing the Dirac points. It is well-established that Dirac cones

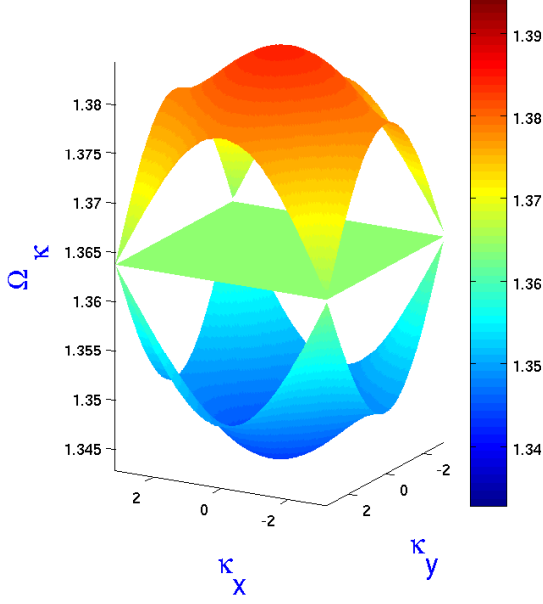


FIG. 3: (Color online) The linear frequency spectrum $\Omega_\kappa(\kappa)$ of the SQUID Lieb metamaterial for $\beta = 0.86$, and $\lambda_x = \lambda_y = -0.02$. The flat-band frequency is $\Omega_{FB} = \Omega_{SQ} \simeq 1.364$.

give rise to peculiar topological properties⁴⁵ and unusual behavior in general, such as effectively massless fermions, etc. Note that the flat-band frequency Ω_{FB} is equal to the resonance frequency of individual SQUIDs Ω_{SQ} , i.e., $\Omega_{FB} = \Omega_{SQ}$. The maximum and minimum frequencies of the spectrum are obtained from Eq. (13) for $\kappa_x = \kappa_y = 0$ and $\kappa_x = \kappa_y = \pi/2$, respectively, as

$$\Omega_{min,max} = \sqrt{\Omega_{SQ}^2 \pm 2\sqrt{\lambda_x^2 + \lambda_y^2}}. \quad (14)$$

Since $|\lambda_x|, |\lambda_y| \ll 1$, the bandwidth of the spectrum is approximately $\Delta\Omega \simeq 2\sqrt{\lambda_x^2 + \lambda_y^2}/\Omega_{SQ}$. For example, for the parameters of Fig. 3 we have $\Omega_{min} \simeq 1.343$, $\Omega_{max} \simeq 1.384$, and $\Delta\Omega \simeq 0.04$. We also note that the flat band is an intrinsic property of this lattice in the nearest-neighbor coupling limit and thus it is not destroyed by any anisotropy (i.e., when $\lambda_x \neq \lambda_y$).

The dependence of the extremal frequencies $\Omega_{min,max}$ and the flat-band frequency Ω_{FB} on the parameters β_L and λ_x, λ_y is shown in Fig. 4. In Fig. 4a all curves increase linearly with increasing β_L while the bandwidth remains practically constant. In Fig. 4b the bandwidth increases with increasing $\lambda_x = \lambda_y$ while Ω_{FB} remains the same.

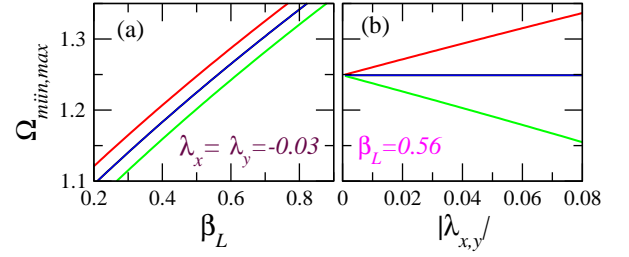


FIG. 4: (Color online) Minimum Ω_{min} (green), maximum Ω_{max} (red), and flat-band frequency Ω_{FB} (blue), as a function of (a) the SQUID parameter β_L for $\lambda_x = \lambda_y = -0.03$, and (b) the coupling coefficients $\lambda_x = \lambda_y$ for $\beta_L = 0.56$.

IV. NUMERICS AND LOCALIZATION MEASURES

The dynamic equations for the fluxes through the SQUIDs, Eqs. (6), without losses and external forcing ($\gamma = 0$ and $\phi_{ext} = 0$), can be derived as the Hamilton's equations from the Hamiltonian function

$$H = \sum_{n,m} H_{n,m}, \quad (15)$$

where the energy (Hamiltonian) density $H_{n,m}$, defined as the energy per unit cell, is given by

$$H_{n,m} = \sum_k \left\{ \frac{\pi}{\beta} \left[(q_{n,m}^k)^2 + (\phi_{n,m}^k)^2 \right] - \cos(2\pi\phi_{n,m}^k) \right\} - \frac{\pi}{\beta} \{ \lambda_x [\phi_{n,m}^A \phi_{n-1,m}^B + 2\phi_{n,m}^A \phi_{n,m}^B + \phi_{n,m}^B \phi_{n+1,m}^A] + \lambda_y [\phi_{n,m}^A \phi_{n,m-1}^C + 2\phi_{n,m}^A \phi_{n,m}^C + \phi_{n,m}^C \phi_{n,m+1}^A] \}, \quad (16)$$

where $q_{n,m}^k = \frac{d\phi_{n,m}^k}{d\tau}$ is the normalized instantaneous voltage across the Josephson junction of the SQUID in the (n,m) th unit cell of kind k . Both H and $H_{n,m}$ are normalized to the Josephson energy, E_J . The total energy H , given by Eqs. (15) and (16), remains constant in time.

Eqs. (6) with $\gamma = 0$ and $\Phi_{ext} = 0$ are integrated in time using the second order symplectic Störmer-Verlet scheme⁴⁶, which preserves the total energy H to a prescribed accuracy which is a function of the time-step h . In the flux - voltage variables, that scheme reads⁴⁶

$$\begin{aligned} \vec{\phi}_{n+\frac{1}{2}}^k &= \vec{\phi}_n^k + \frac{h}{2} \vec{q}_n^k, \\ \vec{q}_{n+1}^k &= \vec{q}_n^k - h H_{\vec{\phi}_n^k}(\vec{\phi}_{n+\frac{1}{2}}^k), \\ \vec{\phi}_{n+1}^k &= \vec{\phi}_{n+\frac{1}{2}}^k + \frac{h}{2} \vec{q}_{n+1}^k, \end{aligned} \quad (17)$$

where $\vec{\phi}^k$ and \vec{q}^k are N -dimensional vectors ($N = N_x N_y$) containing the fluxes and the voltages for the SQUIDs of kind k ($k = A, B, C$), and $H_{\vec{\phi}^k} \equiv \nabla_{\vec{\phi}^k} H$ denotes the column vector of partial derivatives of the

Hamiltonian with respect to $\vec{\phi}^k$, i.e.,

$$H_{\vec{\phi}^k} = \left[\frac{\partial H}{\partial \phi_1^k}, \frac{\partial H}{\partial \phi_2^k}, \frac{\partial H}{\partial \phi_3^k}, \dots, \frac{\partial H}{\partial \phi_N^k} \right]^T.$$

Periodic boundary conditions are used throughout, while the SLiMM is initialized at $\tau = 0$ with a single-site excitation of amplitude A_m . The excited SQUID is either of kind A , B , or C . For isotropic coupling between SQUIDS, i.e., for $\lambda_x = \lambda_y$, a single-site excitation of either a B or a C SQUID provides identical results due to symmetry.

For the identification of the localized states that may be formed either due to the flat band or the nonlinearity, and the quantification of their degree of localization, two statistical measures will be used; the *energetic participation ratio* P_e and the two-dimensional *second moment* M_2 , which are given, respectively, by^{47–49}

$$P_e = \frac{1}{\sum_{n,m} \epsilon_{n,m}^2}, \quad (18)$$

and

$$M_2 = \sum_{n,m} \{(n - \bar{x})^2 + m - \bar{y})^2\} \epsilon_{n,m}, \quad (19)$$

where $\epsilon_{n,m} = H_{n,m}/H$ is the normalized energy density, and \bar{x} , \bar{y} are the coordinates of the "center of energy"

$$\bar{x} = \sum_{n,m} n \epsilon_{n,m}, \quad \bar{y} = \sum_{n,m} m \epsilon_{n,m}. \quad (20)$$

Note that P_e measures roughly the number of excited cells in the system; its values range from $P_e = 1$ (strong localization, all the energy in a single cell) to $P_e = N$, with $N = N_x N_y$ (equipartition of the energy over the N SQUIDS). That measure has been also used to quantify the degree of diffraction in Kagomé photonic lattices⁵⁰. The second moment M_2 quantifies the squared width of the state, hence, its spreading.

Eqs. (6) with $\gamma = 0$ and $\phi_{ext} = 0$, implemented with periodic boundary conditions are initialized with single-site excitations of the form

$$\phi_{n,m}^k(\tau = 0) = \begin{cases} A_m, & \text{if } n = n_e \text{ and } m = m_e; \\ 0, & \text{otherwise,} \end{cases} \quad (21)$$

$$\dot{\phi}_{n,m}^k(\tau = 0) = 0, \text{ for any } n, m, \quad (22)$$

where A_m is the amplitude of the initial excitation, and $k = A, B$ or C . The excited SQUID belongs to the unit cell with $n = n_e, m = m_e$, with $n_e = N_x/2$ and $m_e = N_y/2$. The SLiMM is initialized with A_m spanning several orders of magnitude, and for each A_m several quantities such as the energy, the localization measures, and the ratio $r = |H(\tau) - H(0)|/H(0)$ are monitored during temporal evolution. Typically, a time-step $h = T_{SQ}/1000$, where $T_{SQ} = 2\pi/\Omega_{SQ}$, is used in the simulations. However, it has been checked that smaller time-steps provide practically identical results. It has been also checked that in all runs the ratio r remains less than 5×10^{-6} for the time step h above.

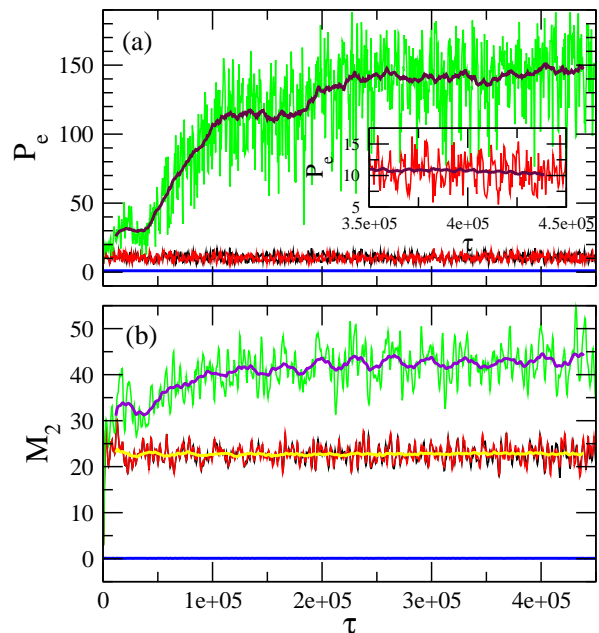


FIG. 5: (Color online) The energetic participation number P_e and the second moment M_2 for a SQUID Lieb lattice with $N_x = N_y = 16$, $\lambda_x = \lambda_y = -0.02$, and $\beta_L = 0.86$ as a function of the normalized time τ . The SQUID of kind C (edge) in the (n_e, m_e) -th cell is initially excited with amplitude A_m . (a) P_e as a function of τ for $A_m = 10^{-3}$ (black); 10^{-2} (red); 10^{-1} (green); 1 (blue). (b) M_2 as a function of τ for $A_m = 10^{-3}$ (black); 10^{-2} (red); 10^{-1} (green); 1 (blue). Inset: P_e as a function of τ for $A_m = 10^{-2}$ and its running average over 5000 T_{SQ} time units.

V. FLAT-BAND AND NONLINEAR LOCALIZATION

The typical time-dependence of P_e and M_2 when an edge SQUID (i.e., a SQUID C) is initially excited with amplitude A_m is shown in Figs. 5a and 5b, respectively, for $A_m = 0.001$ (black), 0.01 (red), 0.1 (green), and 1 (blue). Note that the curves for $A_m = 0.001$ and 0.01 almost coincide; for lower initial amplitudes the results are practically identical to those obtained for $A_m = 0.001$. For such low initial amplitudes the SLiMM remains in the (almost) linear regime, in which localized flat-band states are expected to be observed. Indeed, as can be seen in Fig. 5a, as well as in the inset for $A_m = 0.01$, P_e has a running average over 5000 T_{SQ} time units which is about eleven ($P_e \simeq 11$, inset) indicating substantial localization. The existence of a localized state is advocated in this case by the corresponding second moment M_2 , which running average over 5000 T_{SQ} time units (yellow curve) attains a constant value for relatively long integration times ($M_2 \simeq 22$). The constancy of M_2 is interpreted as the termination of the energy spreading away from the site on which it was initially localized. For $A_m = 0.1$, the inspection of the corresponding (green) curve and its running average (maroon) reveals a dramatic change in

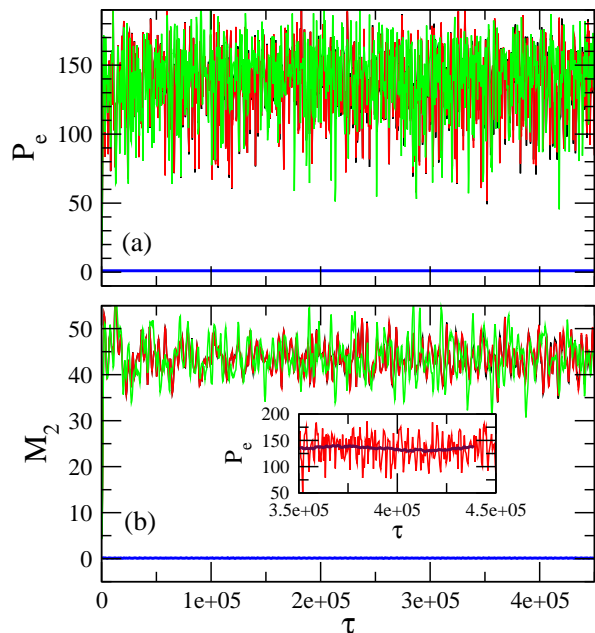


FIG. 6: (Color online) The energetic participation number P_e and the second moment M_2 for a SQUID Lieb lattice with $N_x = N_y = 16$, $\lambda_x = \lambda_y = -0.02$, and $\beta_L = 0.86$ as a function of the normalized time τ . The SQUID of kind A (corner) in the (n_e, m_e) -th cell is initially excited with amplitude A_m . (a) P_e as a function of τ for $A_m = 10^{-3}$ (black); 10^{-2} (red); 10^{-1} (green); 1 (blue). (b) M_2 as a function of τ for $A_m = 10^{-3}$ (black); 10^{-2} (red); 10^{-1} (green); 1 (blue). Inset: P_e as a function of τ for $A_m = 10^{-2}$ and its running average over 5000 T_{SQ} time units.

the behavior of $P_e(\tau)$; the value of the latter increases more or less linearly with increasing τ until it saturates at a rather high value around $P_e \sim 140$. Note however the plateaus in the running average curve which indicate that the SLiMM passes through several metastable states until it reaches the steady one. The second moment M_2 in this case oscillates around 43. Finally, for $A_m = 1$ significant nonlinear effects come into play that favor strong localization with $P_e \sim 1$; thus, all the energy initially provided to the system at a single site, it practically remains there! This is actually the reason why the value of M_2 remains for all times close to zero ($M_2 \simeq 0.1$, there is no spreading of energy whatsoever). Clearly, three different regimes can be identified; the (almost) linear regime, in which flat-band localization is possible, the intermediate regime, in which no localization is observed and the initial energy is eventually spread (in time-scales longer than those shown here) over the whole lattice, and the nonlinear regime in which localization in the form of intrinsically localized modes or discrete breathers, is observed. The size of fluctuations, e.g., in the curves for P_e , depends on that regime which in turn is determined by the initial condition (excitation); thus, fluctuations are weak in the linear, strong in the intermediate, and vanishing in the nonlinear regime.

The corresponding time-dependence of P_e and M_2 when a corner SQUID (i.e., a SQUID A) is initially excited with amplitude A_m is shown in Figs. 6a and 6b, respectively. In this case, there is no localization in the linear and the intermediate regimes, i.e., for $A_m = 0.001$ (black), 0.01 (red), and 0.1 (green), as can be inferred by the large values of P_e whose running average over 5000 T_{SQ} time units is about 140 ($P_e \sim 140$). At the initial stage of time integration which is not visible on the scale of the temporal axis of Fig. 6, both P_e and M_2 have low values; however, within a few thousands time units they gradually grow to their high values. Note that the average of the curves for M_2 (~ 43) is very close to that of the average of the corresponding curve for $A_m = 0.1$ in Fig. 5b (intermediate regime). For high initial amplitude ($A_m = 1$), however, strong localization due to nonlinearity is again observed. For such high values of A_m the localized state which is generated either by initially exciting an A or a C SQUID does not reveal any significant difference. When there is no localization, the fluctuations of both P_e and M_2 are again very strong. The results presented in Figs. 5 and 6 have been obtained for $\lambda_x = \lambda_y$, i.e., in the case of an isotropic Lieb lattice in the nearest-neighbor approximation. In this case, for single-site initial excitations of either a C SQUID or a B SQUID (i.e., of edge SQUIDs), the results are practically identical.

The above scenario is confirmed by inspecting the corresponding energy density plots, i.e., the plots of the energy density $E_{n,m} = H_{n,m}$ on the $n - m$ plane, which are shown in Fig. 7. In Fig. 7a, for $A_m = 0.001$, the energy density $E_{n,m}$ is clearly localized, although not on only one unit cell; the energetic participation ratio is in this case $P_e \simeq 10.5$. A similar pattern is obtained for $A_m = 0.01$, as shown in Fig. 7b, in which the maximum of the energy density is approximately two orders of magnitude larger than that in Fig. 7a. In Fig. 7c, there is clearly no localization, as it can also be inferred by the large participation ratio $P_e \simeq 140$. In Fig. 7d, in which the localization is due to the nonlinearity, the energy is almost completely localized, and $P_e \simeq 1$.

It should be noted that there are particular types of modes which cannot be efficiently excited in the SLiMM with initial single-site excitations used here. As an example, consider the application of the constraint $\phi_{n,m}^A = 0$ for all the SQUIDs of kind A . That case has been also considered in a rhombic (quasi-) one-dimensional system with three waveguides per unit cell, whose coupling functions are the same with those of the equations for the SLiMM³¹. By setting $\phi_{n,m}^A = 0$ for all n and m and $\phi_{n,m}^B = \phi_{n,m}^C = \delta_{n,n_1} \delta_{m,m_1}$, with n_1 and m_1 integers, we get from the first of Eqs. (8) or the first of Eqs. (6) with $\gamma = 0$ and $\phi_{ext} = 0$, that $\lambda_x \phi_{n_1, m_1}^B = -\lambda_y \phi_{n_1, m_1}^C$ ($\phi_{n,m}^B = \phi_{n,m}^C = 0$ for $n \neq n_1$ and $m \neq m_1$). That particular solution for the SLiMM system (either the linearized one or not) certainly cannot be obtained using single-site initial excitations.

In order to roughly determine the boundaries between

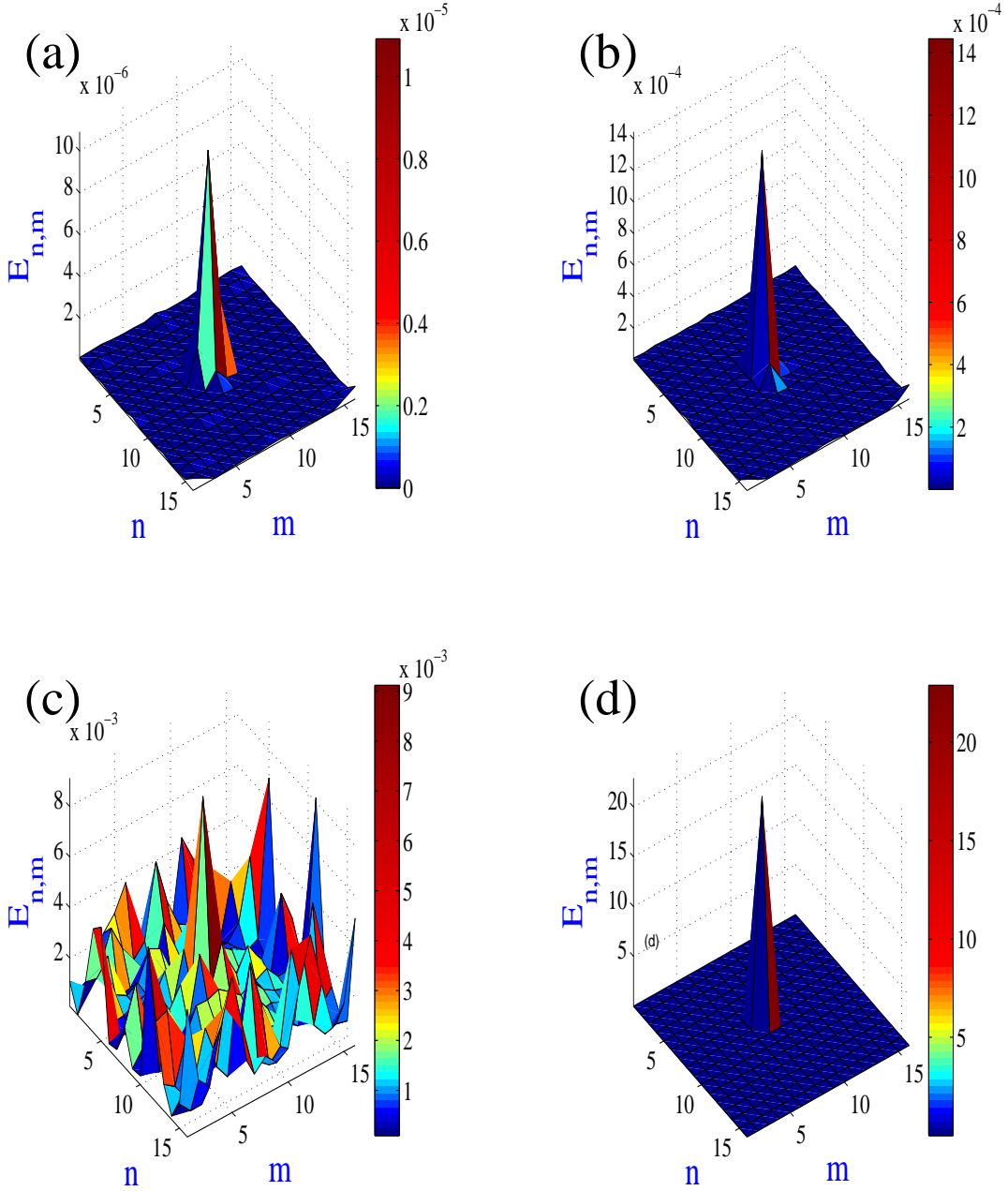


FIG. 7: (Color online) Energy density $E_{n,m} = H_{n,m}$ (energy per unit cell) plotted as a function of n and m , after the equations for the SQUID Lieb metamaterial have been integrated for $10^5 T_{SQ}$ time units. An edge (C) SQUID is initially excited with amplitude $A_m = 0.001$ (a); 0.01 (b); 0.1 (c); 1 (d). Parameters: $N_x = N_y = 16$, $\lambda_x = \lambda_y = -0.02$, and $\beta_L = 0.86$.

the linear, intermediate, and nonlinear regimes, the averages of several quantities over the *steady-state integration time* τ_{int} were calculated for a wide range of initial excitation amplitudes $A_m = A_{m,i}$. An edge (C) SQUID is initially excited with amplitude $A_{m,i}$ and Eqs. (6) with $\gamma = 0$ and $\phi_{ext} = 0$ are integrated in time for $\tau_{int} = 10^5 T_{SQ}$ time units, to allow for transients to die out (the obtained results are discarded) and the steady state to be reached. Then, in the steady state, the equations are integrated in time for τ_{int} more time units,

and the energetic participation ratio averaged over τ_{int} is calculated. At the end of the steady-state integration time, the amplitude of the flux of the excited SQUID, $A_{m,c}$, and the oscillation frequency of the flux through the loop of the excited SQUID, Ω_{osc} , are also calculated. The same calculations are performed for an initially excited corner SQUID A , and the results for both cases are shown in Fig. 8. In Fig. 8a, the calculated amplitude $A_{m,c}$ of the flux ϕ_{n_e, m_e}^k through the loop of the SQUID with $k = A$ (blue) and $k = C$ (green) is shown along

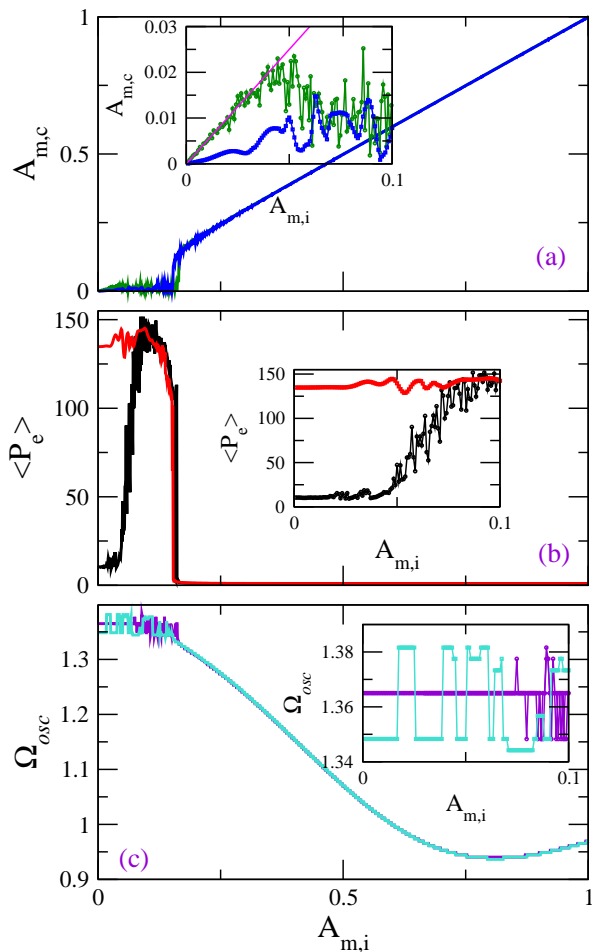


FIG. 8: (Color online) (a) The amplitude $A_{m,c}$ of the flux ϕ_{n_e, m_e}^k of the initially excited SQUIDs with $k = A$ (blue curve) and $k = C$ (green curve) calculated at the end of the integration time as a function of the initial excitation amplitude $A_{m,i}$. Inset: Enlargement around low $A_{m,i}$. The line $A_{m,i}/2$ is shown in magenta color. (b) The energetic participation ratio averaged over the integration time, $\langle P_e \rangle$, (transients were discarded) for the SQUID Lieb metamaterial when a corner (A) SQUID (red curve) and an edge (C) SQUID (black curve) is initially excited, as a function of the initial excitation amplitude $A_{m,i}$. (c) The oscillation frequency Ω_{osc} of the flux ϕ_{n_e, m_e}^k of the initially excited $k = A$ (violet curve) and $k = C$ (turquoise curve) SQUID as a function of the initial excitation amplitude $A_{m,i}$. Parameters: $N_x = N_y = 16$, $\lambda_x = \lambda_y = -0.02$, and $\beta_L = 0.86$.

with an enlargement for low $A_{m,i}$ (inset). As it can be observed, $A_{m,c}$ attains low values for low initial amplitudes $A_{m,i} < 0.15$, while for $A_{m,i} > 0.15$ the calculated amplitude $A_{m,c}$ increases linearly with increasing $A_{m,i}$, according to the approximate relation $A_{m,c} \simeq A_{m,i}$. The behavior for $A_{m,i} > 0.15$ is a result of the strong localization taking place due to nonlinearities and it does not depend on which kind of SQUID (edge or corner) is initially excited. However, a closer look to the two curves for $A_{m,i} < 0.15$, reveals significant differences, especially

for $A_{m,i} < 0.05$, which can be seen more clearly in the inset. In this regime the calculated amplitude $A_{m,c}$ for $k = C$ follows the relation $A_{m,c} \simeq A_{m,i}/2$, indicating localization due to the flat band. This conclusion is also supported by Figs. 8b and 8c. In Fig. 8b, the energetic participation ratio averaged over τ_{int} , $\langle P_e \rangle$, for low values of $A_{m,i}$ attains very different values depending on which kind of SQUID is initially excited (A or C); specifically, while $\langle P_e \rangle \sim 10.5$ for the SLiMM when a C SQUID is initially excited (black), it is $\langle P_e \rangle \sim 140$ when an A SQUID is initially excited (red). That large difference between the values of $\langle P_e \rangle$ is due to flat-band localization in the former case and delocalization in the latter case since no flat-band modes are excited. In the inset, it can be observed that $\langle P_e \rangle$ for an initially excited C SQUID starts increasing for $A_{m,i} > 0.05$ indicating gradual degradation of flat-band localization and meets the $\langle P_e \rangle$ curve for an initially excited A SQUID at $A_{m,i} \sim 0.1$. In Fig. 8c, for $A_{m,i} < 0.15$, the oscillation frequency of the flux through the initially excited SQUID Ω_{osc} (either A or C), has a value around that of the linear resonance frequency of a single SQUID, Ω_{SQ} ($\Omega_{SQ} \simeq 1.364$ for the parameters of Fig. 8). As it can be seen in the inset, when a C SQUID is initially excited (violet), then up to high accuracy $\Omega_{osc} = \Omega_{SQ}$ for initial amplitudes up to $A_{m,i} \sim 0.075$. However, when an A SQUID is initially excited (turquoise), the frequency Ω_{osc} jumps slightly above and below Ω_{SQ} irregularly, but it remains within the bandwidth of the linear frequency spectrum. For $A_{m,i} > 0.15$, the frequency Ω_{osc} decreases with increasing $A_{m,i}$, although it starts increasing again with increasing $A_{m,i}$ at $A_{m,i} \sim 0.8$. In this regime, nonlinear localized modes of the breather type are formed, which frequency lies outside the linear frequency spectrum and depends on its amplitude, as it should be. From this figure it can thus be inferred that flat-band localization occurs for initial amplitudes up to $A_{m,i} \simeq 0.05$ (linear regime), while delocalization occurs in the interval $0.05 < A_{m,i} < 0.15$ (intermediate regime). For larger $A_{m,i}$, strong nonlinear localization occurs (nonlinear regime). This rough estimation for the boundaries between the three regimes is of course parameter dependent. Remarkably, flat-band localization occurs only when an edge SQUID (B or C) is initially excited. The excitation of a corner (A) SQUID does not lead to excitation of flat-band modes and thus such a localized initial state rapidly delocalizes. On the other hand, the observed flat-band localization is not very strong as compared to the nonlinear localization. This is probably due to the fact that a single-site excitation of a B or C SQUID does not correspond to an exact localized flat-band eigenmode.

In the case of anisotropic coupling, i.e., for $\lambda_x \neq \lambda_y$, single-site excitations of B and C SQUIDs give different results as expected due to the lowering of symmetry³⁷. Typical curves for the amplitude of the flux ϕ_{n_e, m_e}^k of the excited SQUID $A_{m,c}$ ($k = A, B$, and C), the energetic participation ratio averaged over the steady-state

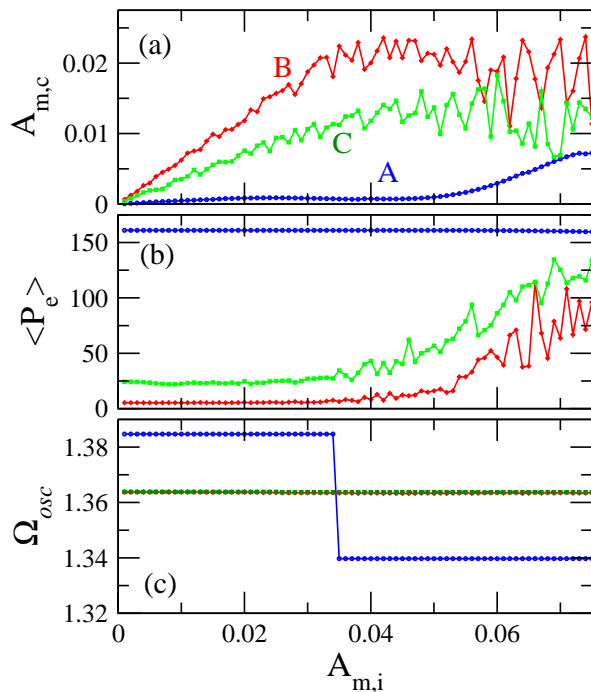


FIG. 9: (Color online) (a) The amplitude $A_{m,c}$ of the fluxes ϕ_{n_e, m_e}^k of the excited SQUIDs with $k = A$ (black), B (red), and C (green), in the (n_e, m_e) th unit cell, calculated at the end of the integration time as a function of relatively low initial excitation amplitudes $A_{m,i}$; (b) the corresponding energetic participation ratio $i < P_e >$ averaged over the steady-state integration time τ_{int} (transients were discarded), and (c) the corresponding oscillation frequency Ω_{osc} of the fluxes ϕ_{n_e, m_e}^k , for $N_x = N_y = 16$, $\beta_L = 0.86$, and anisotropic coupling $\lambda_x = -0.02$, $\lambda_y = -0.03$.

integration time $\langle P_e \rangle$, and the oscillation frequency Ω_{osc} of the flux through the excited SQUID, are shown in Fig. 9 for anisotropic nearest-neighbor coupling, $\lambda_y = 1.5\lambda_x = -0.03$, as a function of relatively low initial excitation amplitudes $A_{m,i}$ for which flat-band localization is expected. As can be observed in Fig. 9a, flat-band localization occurs when either of the edge SQUIDs are excited with $A_{m,i} < 0.04$. For larger values of $A_{m,i}$, localization starts degrading as it can be confirmed from the corresponding curves of $\langle P_e \rangle$ in Fig. 9b. Here, it is also apparent that initial excitations of B and C SQUIDs do not lead to a state with the same degree of localization; indeed, $\langle P_e \rangle$ is respectively ~ 5 and ~ 25 (while the corresponding $\langle P_e \rangle$ for initial excitations of an A SQUID is about 160). The corresponding oscillation frequencies of the fluxes in the case of B or C SQUID initial excitations are practically equal to that of the single SQUID resonance $\Omega_{SQ} \simeq 1.364$. For initial excitations of an A SQUID, the oscillation frequency is very close to that of either the upper or the lower boundary of the linear frequency spectrum.

VI. CONCLUSIONS

The dynamic equations for the fluxes threading the SQUID loops of a driven-dissipative SLiMM have been derived, along with the corresponding linear frequency spectrum. The Lieb lattice geometry results in a spectrum with two dispersive bands, which form a Dirac cone at the corners of the first Brillouin zone, and a flat band crossing those Dirac points. The localization properties of Hamiltonian SLiMMs, i.e., those without dissipation and driving terms, have been determined through numerical simulations for single-site initial excitations of varying amplitude. Flat-band localization, i.e., the emergence of localized flat-band states, is observed when an edge (B or C) SQUID of the unit cell of the SLiMM is initially excited with low amplitude. To the contrary, no such states are generated when a corner (A) SQUID of the unit cell of the SLiMM is initially excited with low amplitude. These results are compatible with the experiments on photonic Lieb lattices³³. For sufficiently high amplitude of the initial excitation of either a corner or an edge SQUID, localization due to nonlinearities in the form of discrete breathers is observed. The linear (low amplitude initial excitations) and the nonlinear regimes (high amplitude initial excitations), in which flat-band localized states and discrete breathers, respectively, can be generated, are separated by an intermediate regime in which neither type of localization is observed. This dynamic behavior is quite different from that observed in, e.g., two-dimensional Kagomé lattices in which families of nonlinear localized modes in the form of discrete solitons or discrete breathers may bifurcate from localized linear modes of the flat band^{39,40}. Here, relatively high-amplitude initial excitations ($A_{m,i} > 0.05$) excite nonlinear effects in the SQUIDs which destroy the flatness of the flat-band which has been obtained in the linear limit. At the same time, however, these nonlinear effects are not strong enough to help the initial excitation to remain localized (self-trapped); that occurs only when the amplitude of the initial excitation exceeds a particular, parameter-dependent threshold ($A_{m,i} \simeq 0.15$ for the parameters of Fig. 8).

ACKNOWLEDGMENT

This work is partially supported by the Ministry of Education and Science of the Russian Federation in the framework of the Increase Competitiveness Program of NUST "MISiS" (No. K2-2015-007) and by the Ministry of Education and Science of the Republic of Kazakhstan (Contract # 339/76 -2015). NL gratefully acknowledges the Laboratory for Superconducting Metamaterials, NUST "MISiS" for its warm hospitality during visits.

- ¹ D. R. Smith, J. B. Pendry, and Wiltshire, Metamaterials and negative refractive index, *Science* **305**, 788 (2004).
- ² T. J. Yen, W. J. Padilla, N. Fang, D. C. Vier, D. R. Smith, J. B. Pendry, D. N. Basov, and X. Zhang, Terahertz magnetic response from artificial materials, *Science* **303**, 1494 (2004).
- ³ S. Linden, C. Enkrich, G. Dolling, M. W. Klein, J. Zhou, T. Koschny, C. M. Soukoulis, S. Burger, F. Schmidt, and M. Wegener, Magnetic response of metamaterials at 100 terahertz, *Science* **306**, 1351 (2004).
- ⁴ S. Linden, C. Enkrich, G. Dolling, M. W. Klein, J. Zhou, T. Koschny, C. M. Soukoulis, S. Burger, F. Schmidt, and M. Wegener, Photonic metamaterials: magnetism at optical frequencies, *IEEE J. Sel. Top. Quant. Electron.* **12**, 1097 (2006).
- ⁵ V. M. Shalaev, Optical negative-index metamaterials, *Nature Photon.* **1**, 41 (2007).
- ⁶ N. M. Litchinitser and V. M. Shalaev, Photonic metamaterials, *Laser Phys. Lett.* **5**, 411 (2008).
- ⁷ A. D. Boardman, V. V. Grimalsky, Y. S. Kivshar, S. V. Koshevaya, M. Lapine, N. M. Litchinitser, V. N. Malnev, M. Noginov, Y. G. Rapoport, and V. M. Shalaev, Active and tunable metamaterials, *Laser Photonics Rev.* **5**, 287 (2010).
- ⁸ Y. S. Kivshar, M. Lapine, I. V. Shadrivov, Colloquium: Nonlinear metamaterials, *Rev. Mod. Phys.* **86**, 1093 (2014).
- ⁹ N. I. Zheludev, The road ahead for metamaterials, *Science* **328**, 582 (2010).
- ¹⁰ N. I. Zheludev, A roadmap for metamaterials, *Optics and Photonics News* **22**, 31 (2011).
- ¹¹ N. I. Zheludev and Yu. S. Kivshar, From metamaterials to metadevices, *Nature Mater.* **11**, 917 (2012).
- ¹² S. M. Anlage, The physics and applications of superconducting metamaterials, *J. Opt.* **13**, 024001 (2011).
- ¹³ P. Jung, A. V. Ustinov, and S. M. Anlage, Progress in superconducting metamaterials, *Supercond. Sci. Technol.* **27**, 073001 (2014).
- ¹⁴ C. Du, H. Chen, and S. Li, Quantum left-handed metamaterial from superconducting quantum-interference devices, *Phys. Rev. B* **74**, 113105 (2006).
- ¹⁵ N. Lazarides and G. P. Tsironis, rf superconducting quantum interference device metamaterials, *Appl. Phys. Lett.* **90**, 163501 (2007).
- ¹⁶ B. Josephson, Possible new effects in superconductive tunnelling, *Phys. Lett. A* **1**, 251 (1962).
- ¹⁷ P. Jung, S. Butz, S. V. Shitov, and A. V. Ustinov, Low-loss tunable metamaterials using superconducting circuits with Josephson junctions, *Appl. Phys. Lett.* **102**, 062601 (2013).
- ¹⁸ S. Butz, P. Jung, L. V. Filippenko, V. P. Koshelets, and A. V. Ustinov, A one-dimensional tunable magnetic metamaterial, *Opt. Express* **21**, 22540 (2013).
- ¹⁹ M. Trepanier, Daimeng Zhang, O. Mukhanov, and S. M. Anlage, Realization and modeling of rf superconducting quantum interference device metamaterials, *Phys. Rev. X* **3**, 041029 (2013).
- ²⁰ Daimeng Zhang, M. Trepanier, O. Mukhanov, and S. M. Anlage, Broadband transparency of macroscopic quantum superconducting metamaterials, *Phys. Rev. X* **5**, 041045 (2015).
- ²¹ P. Jung, S. Butz, M. Marthaler, M. V. Fistul, J. Leppäkangas, V. P. Koshelets, and A. V. Ustinov, Multistability and switching in a superconducting metamaterial, *Nat. Comms.* **5**, 3730 (2014).
- ²² N. Lazarides and G. P. Tsironis, Multistability and self-organization in disordered SQUID metamaterials, *Supercond. Sci. Technol.* **26**, 084006 (2013).
- ²³ G. P. Tsironis, N. Lazarides, and I. Margaritis, Wide-band tuneability, nonlinear transmission, and dynamic multistability in SQUID metamaterials, *Appl. Phys. A* **117**, 579 (2014).
- ²⁴ N. Lazarides, G. P. Tsironis, and M. Eleftheriou, Dissipative discrete breathers in rf SQUID metamaterials, *Nonlinear Phenom. Complex Syst.* **11**, 250 (2008).
- ²⁵ N. Lazarides, G. Neofotistos, and G. P. Tsironis, Chimeras in SQUID metamaterials, *Phys. Rev. B* **91**, 054303 (2015).
- ²⁶ J. Hizanidis, N. Lazarides, and G. P. Tsironis, Robust chimera states in SQUID metamaterials with local interactions, *Phys. Rev. E* **94**, 032219 (2016).
- ²⁷ C. Danieli, J. D. Bodyfelt, and S. Flach, Flat-band engineering of mobility edges, *Phys. Rev. B* **91**, 235134 (2015).
- ²⁸ R. Khomeriki and S. Flach, Landau-Zener Bloch oscillations with perturbed flat bands, *Phys. Rev. Lett.* **116**, 245301 (2016).
- ²⁹ D. Leykam, S. Flach, O. Bahat-Treidel, and A. S. Desyatnikov, Flat band states: Disorder and nonlinearity, *Phys. Rev. B* **88**, 224203 (2013).
- ³⁰ D. Leykam, J. D. Bodyfelt, A. S. Desyatnikov, and S. Flach, Localization of weakly disordered flat band states, *Eur. Phys. J. B* **90**, 1 (2017).
- ³¹ A. I. Maimistov, On the stability of flat-band modes in a rhombic nonlinear optical waveguide array, *J. Opt.* **19**, 045502 (2017).
- ³² D. Leykam, O. Bahat-Treidel, and A. S. Desyatnikov, Pseudospin and nonlinear conical diffraction in Lieb lattices, *Phys. Rev. A* **86**, 031805(R) (2012).
- ³³ S. Mukherjee, A. Spracklen, D. Choudhury, N. Goldman, P. Öhberg, E. Andersson, and R. R. Thomson, Observation of a localized flat-band state in a photonic Lieb lattice, *Phys. Rev. Lett.* **114**, 245504 (2015).
- ³⁴ R. A. Vicencio, C. Cantillano, L. Morales-Inostroza, B. Real, C. Mejía-Cortés, S. Weimann, A. Szameit, and M. I. Molina, Observation of localized states in Lieb photonic lattices, *Phys. Rev. Lett.* **114**, 245503 (2015).
- ³⁵ Liu Zheng, Liu Feng, and Wu Yong-Shi, Exotic electronic states in the world of flat bands: From theory to material, *Chin. Phys. B* **23**, 077308 (2014).
- ³⁶ M. R. Slot, T. S. Gardenier, P. H. Jacobse, G. C. P. van Miert, S. N. Kempkes, S. J. M. Zevenhuizen, C. Morais Smith, D. Vanmaekelbergh, and I. Swart, Experimental realization and characterization of an electronic Lieb lattice, *Nature Phys.* **1**, 1 (2017).
- ³⁷ D. Guzmán-Silva, C. Mejía-Cortés, M. A. Bandres, M. C. Rechtsman, S. Weimann, S. Nolte, M. Segev, A. Szameit, and R. A. Vicencio, Experimental observation of bulk and edge transport in photonic Lieb lattices, *New J. Phys.* **16**, 063061 (2014).
- ³⁸ S. Flach and A. V. Gorbach, Discrete breathers - advances in theory and applications, *Phys. Rep.* **467**, 1 (2008).
- ³⁹ R. A. Vicencio and M. Johansson, Discrete flat-band solitons in the Kagomé lattice, *Phys. Rev. A* **87**, 061803(R) (2013).

- (2013).
- ⁴⁰ M. Johansson, U. Naether, and R. A. Vicencio, Compactification tuning for nonlinear localized modes in sawtooth lattices, *Phys. Rev. E* **92**, 032912 (2015).
- ⁴¹ P. P. Belicev, G. Gligorić, A. Radosavljevic, A. Maluckov, M. Štepic, R. A. Vicencio, and M. Johansson, Localized modes in nonlinear binary Kagomé ribbons, *Phys. Rev. E* **92**, 052916 (2015).
- ⁴² D. López-González and M. I. Molina, Linear and nonlinear compact modes in quasi-one-dimensional flatband systems, *Phys. Rev. A* **93**, 043847 (2016).
- ⁴³ G. Gligorić, A. Maluckov, Lj. Hadzievski, S. Flach, and B. A. Malomed, Nonlinear localized flat-band modes with spin-orbit coupling, *Phys. Rev. B* **94**, 144302 (2016).
- ⁴⁴ K. K. Likharev, *Dynamics of Josephson Junctions and Circuits*, Gordon and Breach, Philadelphia, 1986.
- ⁴⁵ C. Weeks and M. Franz, Topological insulators on the Lieb and perovskite lattices, *Phys. Rev. B* **82**, 085310 (2010).
- ⁴⁶ E. Hairer, C. Lubich, and G. Wanner, Geometric numerical integration illustrated by the Störmer-Verlet method, *Acta Numerica* **2003**, 399 (2003).
- ⁴⁷ T. V. Lapyeva, J. D. Bodyfelt, and S. Flach, Subdiffusion of nonlinear waves in two-dimensional disordered lattices, *Europhys. Lett.* **98**, 60002 (2012).
- ⁴⁸ M. Mulansky and A. Pikovsky, Scaling properties of energy spreading in nonlinear Hamiltonian two-dimensional lattices, *Phys. Rev. E* **86**, 056214 (2012).
- ⁴⁹ F. A. B. F. de Moura, M. D. Coutinho-Filho, E. P. Raposo, and M. L. Lyra, Delocalization in harmonic chains with long-range correlated random masses, *Phys. Rev. B* **68**, 012202 (2003).
- ⁵⁰ R. A. Vicencio and C. Mejía-Cortés, Diffraction-free image transmission in Kagomé photonic lattices, *J. Opt.* **16**, 015706 (2014).